16th World Conference on Earthquake Engineering, 16WCEE 2017
Santiago Chile, January 9th to 13th 2017
Paper N° 2104 (Abstract ID)
Registration Code: S-L1465292083

A TSUNAMI PROPAGATION MODELING BASED ON THE ADAPTIVE MESH REFINEMENT

T. Maeda[(1)], S. Aoi[(2)], A. Iwaki[(3)], and T. Hayakawa[(4)]

[(1)] Senior Researcher, National Research Institute for Earth Science and Disaster Resilience, tmaeda@bosai.go.jp
[(2)] Director, National Research Institute for Earth Science and Disaster Resilience, aoi@bosai.go.jp
[(3)] Research Fellow, National Research Institute for Earth Science and Disaster Resilience, iwaki@bosai.go.jp
[(4)] Group Manager, Mitsubishi Space Software Co., ltd., Hayakawa.Toshihiko@mss.co.jp

Abstract

We develop an automatic system for generating the optimal mesh model based on the adaptive mesh refinement method and the tsunami propagation simulation code adapted for the adaptive mesh model. The adaptive mesh is constructed by discretizing a domain spatially using tree-structure grid (quad-tree and nona-tree grids). Developed simulation code is compared with the conventional tsunami simulation code. The simulation results for the same bathymetry and source data show good agreement. The number of grid cell of the adaptive mesh model is about half that of a uniform mesh model. And the calculation time of the developed code is shorter than that of the conventional code with a uniform grid by approximately 10%. The parallelization efficiency of the developed code adapted for the non-linear long-wave theory applied to the nona-tree grid model with four consolidation level is around 70% in the case of 24 parallel-running tasks.

Keywords: Tsunami; Adaptive mesh refinement; Tree-structure grid

1. Introduction

For improving a tsunami hazard assessment, it is important to understand a possible range of tsunami inundation as well as tsunami height caused by uncertainty of source model. Simulations based on many possible source models are necessary to take into account the variety in the source model. Thus an efficient tsunami inundation simulation is especially important. For the efficient tsunami modeling, reduction of the number of grid cells is effective. To reduce the total number of grid cells, it is important to construct a mesh model with the most suitable grid spacing according to the bathymetry and connect the grid cells appropriately because the grid spacing depends on a propagation speed of tsunamis. A nesting is usually employed as the method to connect the grid cells. The nesting, however, has difficulty in constructing the most suitable grid spacing because regions for finer grid spacing are determined manually. Therefore, in this study, we developed a system to automatically generate an optimal mesh model based on the adaptive mesh refinement (AMR) method and a tsunami propagation calculation code adapted for the AMR.

2. Construction of adaptive mesh model

We employ the AMR by discretizing a domain spatially using tree-structure grid (quad-tree and nona-tree grids). In the AMR method, structured grids are consolidated based on the local tsunami propagation speed. The tree-structure grid was applied to the tsunami simulation in previous studies (e.g., [1, 2, 3, 4, 5]). In these studies, quad-tree structure, in which grid cell is dividing into four grids of 2×2, is used. In this study, in addition to the quad-tree structured grid, nona-tree structured grid which divides cell into nine grids of 3×3 is also adopted. The quad-tree grid has advantage in easy creation of data structure, while the nona-tree structured grid has advantage in using bathymetry data created for the nesting: the bathymetry data for the nesting are prepared with several different grid spacing and their size ratio is usually 3:1.

The adaptive meshes are automatically created by consolidating bathymetry data in the minimum grid spacing based on ①Courant-Friedrichs-Lewy (CFL) condition, ② numerical dispersion conditions, ③ forced consolidation conditions, and ④ adjacent-level conditions. ① and ② can be represented by the following equations as,

$$1 > \alpha_{CFL} \frac{\Delta t}{\Delta x} \sqrt{2gh} \tag{1}$$

$$\Delta x = \Delta x_0 \times I^l < \frac{T}{\alpha_T} \sqrt{gh} \tag{2}$$

where α_{CFL} is the factor of safety, Δt is the time interval, Δx is the grid spacing, h is the water depth, Δx_0 is the initial (minimum) grid spacing, I is 2 (quad-tree) or 3 (nona-tree), l is the consolidation level, T is the period of the tsunami, and α_T is the minimum number of grids within a unit wavelength. Minimum grid spacing is found so that it satisfies these conditions. ③ is a condition for two kinds of regions. One is the regions where water does not reach since their altitudes are sufficiently high. An appropriate altitude value is given as a threshold. It can reduce the number of grid cells by forcing the grid to be maximum spacing. Another is the regions where the conditions of ① and ② are satisfied but grid spacing is smaller than its neighbors (yellow cells in Fig 1b). Grid cells in these regions are consolidated so that the grid spacing is similar to the surroundings. ④ is a condition for smoothing the consolidation level of the adjacent grid to avoid the level to be skipped a two or more between neighbors (red cells in Fig 1b). This condition is based on the previous study [1]. Finally, the grid coordinates of the lower left (southwest corner) are given to the consolidated mesh. Further, the physical quantity within the final grid cell is represented by the average value of all the original grids contained in the final grid cell. Each grid cell is numbered. And x coordinate, y coordinate, consolidation-level information, and grid number of the adjacent grid cell are associated with the grid number of corresponding cell.

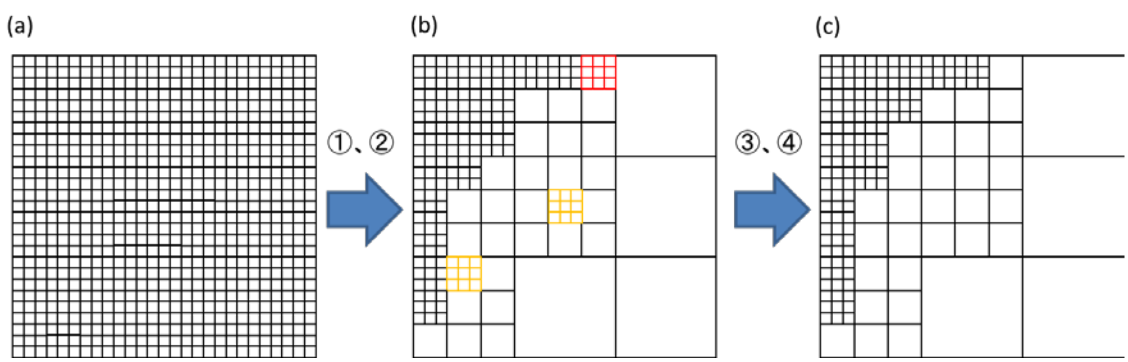

Fig. 1 Schematic of constructing adaptive meshes. Explanation of ①~④ is shown in the text. Uniform grids (a) are consolidated based on the conditions ① and ②. Then, yellow and red cells in (b) are consolidated based on the conditions ③ and ④, respectively.

The number of total grid cells due to AMR method is compared to that due to conventional nesting method (Fig.2). Along the coastal area the Sea of Japan, the mesh refinement is being carried out by AMR method, the nesting has not been the subject of a subdivision. While the difference of the number of grid cells is smaller when the grid spacing is large (1350m), the number of grid cells by AMR method is at about 1/4 of that of nesting when the grid spacing is small (150m, 50m).

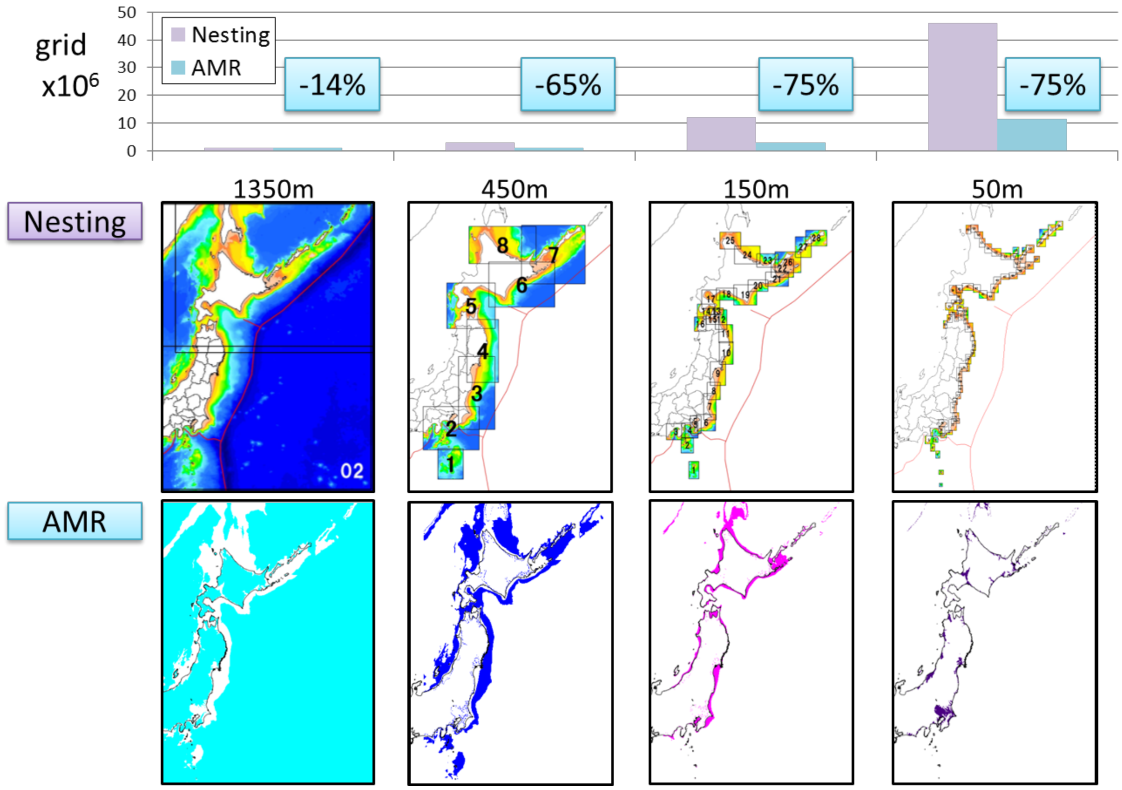

Fig. 2 Upper: comparison of the number of grid cells between AMR and nesting. Lower: the distribution of grid cells for each grid spacing (1350m, 450m, 150m, and 50m). The grid cells of same size are arranged within a rectangular area in the nesting and within a colored area in the AMR.

3. Tsunami propagation simulation

3.1 Calculation scheme

We developed a tsunami propagation simulation code adapted for the AMR based on the linear long-wave theory and non-linear long-wave theory. Our tsunami modeling uses a staggered leap-frog scheme with second-order accuracy. Advection term of the non-linear long-wave theory is treated as upwind difference scheme to eliminate the numerical dispersion. Boundary condition between land and water is a total reflection for the linear long-wave theory, while a run up is taken into consideration by using the Manning's roughness in the boundary condition for the non-linear long-wave theory. Structures are modeled as lines and the Hom-ma formula is used when water overflows them. Boundary condition of the open sea is calculated on the basis of [6], the determination of the open sea in each region boundary is carried out automatically.

3.2 Connection of grid cells

It is needed to connect water level and discharge flux between the meshes with different grid spacing. Linear interpolation between neighboring grids is used if the grid of interest is in contact with the boundary of the computational domain, and a second-order Lagrange polynomial interpolation by three adjacent grids is used to the other region. Here, we show an example of connection of water level by the second-order interpolation in the case of the quad-tree structured grid and nona-tree structured grid. In view of the symmetry, there are three patterns of connection as shown in Fig.3. Since water level is defined at the center of grid cell, the water level of the position marked with blue and red circles in Fig. 3 are obtained using the water level of the grid cells numbered ①, ②, and ③. In Fig. 4, the quadratic curve $F(x)$ passing through three points, ① (x_1, F_1), ②(x_2, F_2), and ③ (x_3, F_3), is expressed by Eq. (3) by the Lagrange interpolation.

$$F(x) = \frac{(x - x_2)(x - x_3)}{(x_1 - x_2)(x_1 - x_3)} F_1 + \frac{(x - x_1)(x - x_3)}{(x_2 - x_1)(x_2 - x_3)} F_2 + \frac{(x - x_1)(x - x_2)}{(x_3 - x_1)(x_3 - x_2)} F_3 \tag{3}$$

suppose a, b,and c are positive integer, and w is a grid spacing for lower region, $F(x_-)$ and $F(x_+)$ are expressed as Eq. (4),

$$F(x_\pm) = \frac{c^2 \mp bc}{a(a+b)} F_1 - \frac{(c \pm a)(c \mp b)}{ab} F_2 + \frac{c^2 \pm ac}{(a+b)b} F_3 \qquad \text{(Double sign correspondence)} \tag{4}$$

By substituting a, b, and c values corresponding to the three cases shown in Fig.3 into Eq. (4), the water level at the blue and red circles is calculated. Incidentally, the water level determined here is used to calculate a discharge flux. The discharge flux is defined at the boundary of the grid cell, it is calculated from the difference between the water level in the blue (red) open circle and blue (red) solid circle in Fig.3.

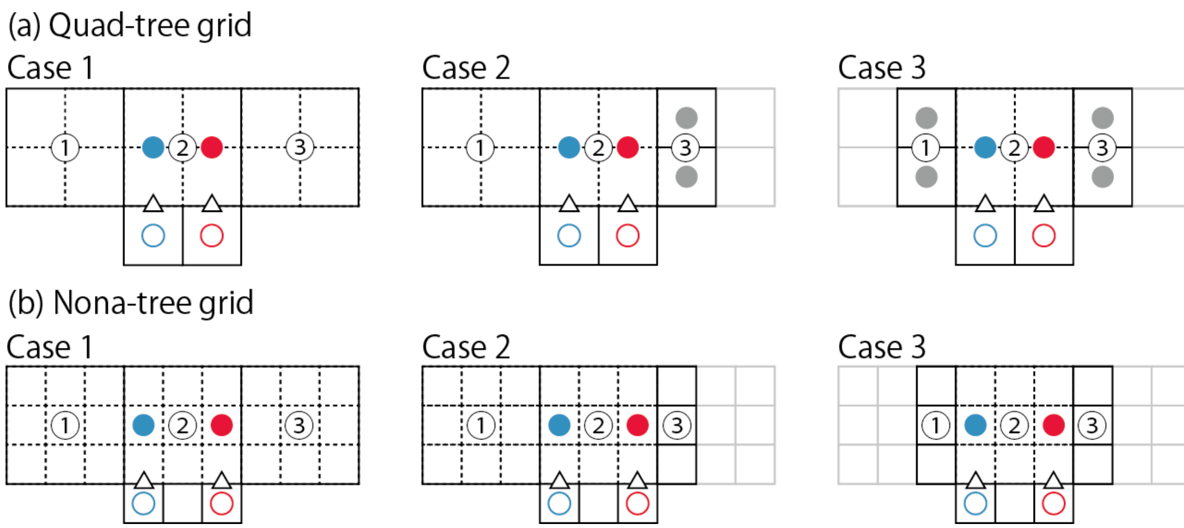

Fig. 3 Example for obtaining water level at blue and red solid circles by the second-order interpolation using the water level defined at the position of ①, ②, and ③. Black thick line is grid boundary and black dotted line indicates the grid boundary before the consolidation. In the quad-tree grid, water level at ③ for case 2 and that at ① and ③are defined by taking average of values at gray circles. It should be noted that the discharge flux at the position of open triangles, is calculated from the respective solid and open circles.

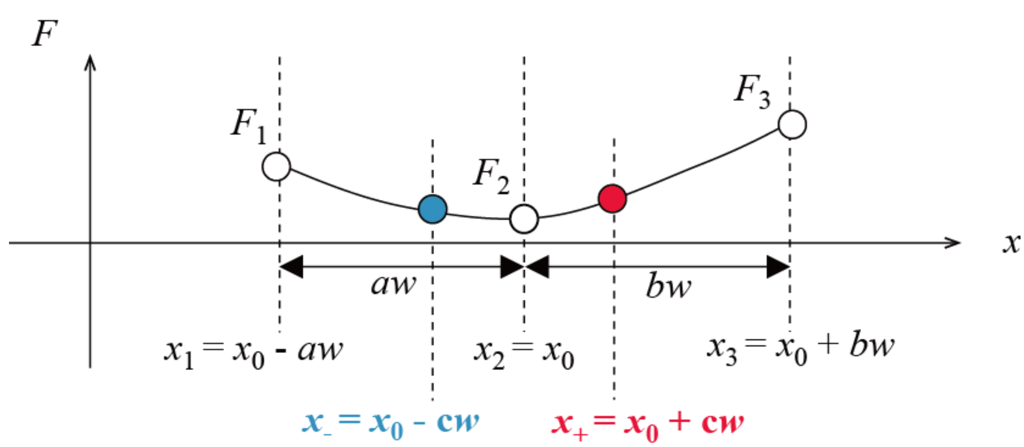

Fig. 4 Schematic of second-order Lagrange interpolation by three adjacent grids.

4. Performance tests

Using a conventional tsunami solver adapted for the uniform grid (hereinafter abbreviated as the conventional solver) and tsunami solver that corresponds to the AMR that was developed in this study (hereinafter abbreviated as AMR solver), we compare the simulation results for the same input data such as source model and bathymetry. Fig. 5 shows the bathymetry and the source model used for the calculation. The circular island is placed at slightly northwest from the center of the computational domain, and the source represented by rectangular fault is placed at southeast from the center. Uniform grid spacing of 450m is used for the conventional solver, and the adaptive mesh model with two consolidation level of 450m/1350m by nona-tree structured grid is used for the AMR solver. Conditions of the automatic creation of adaptive meshes are shown in Table 1. The initial tsunami height is determined based on [7] under the conditions shown in Table 2. Table 3 shows the condition of the tsunami simulation using the conventional solver and AMR solver. It is shown here as an example of the simulation by the non-linear long-wave theory. When comparing the conventional solver and AMR solver by the tsunami waveform and a snapshot of the wave height distribution (Fig. 6), although small differences in the short-wavelength component are recognized, both can be judged to have almost the same. With respect to the computational performance, the number of grid cells is almost half compared with the uniform grid and AMR solver has a shorter calculation time by about 10 %.

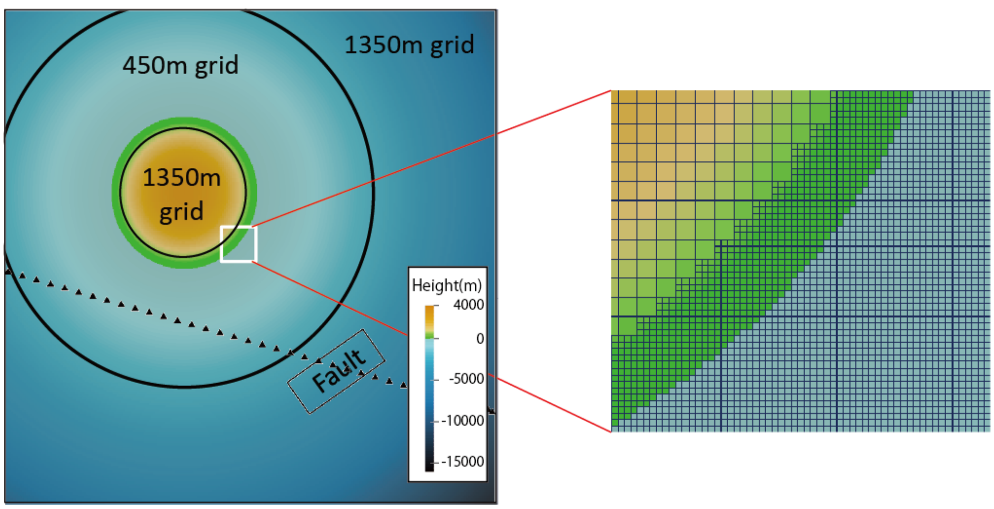

Fig. 5 Left: batymetry and location of the fault and stations (solid triangles) used in the simulation. Two large circles show boundary for regions of different grid spacing in the AMR model. Right: distribution of AMR grid cells.

Table 1 –Setting of the AMR

Parameters	value	Unit
Tree-structure	Nona-tree	
Factor of safety (α_{CFL})	10	
Altitude for the forced consolidation condition	50	m
Period of tsunami	60	s
α_T	6	

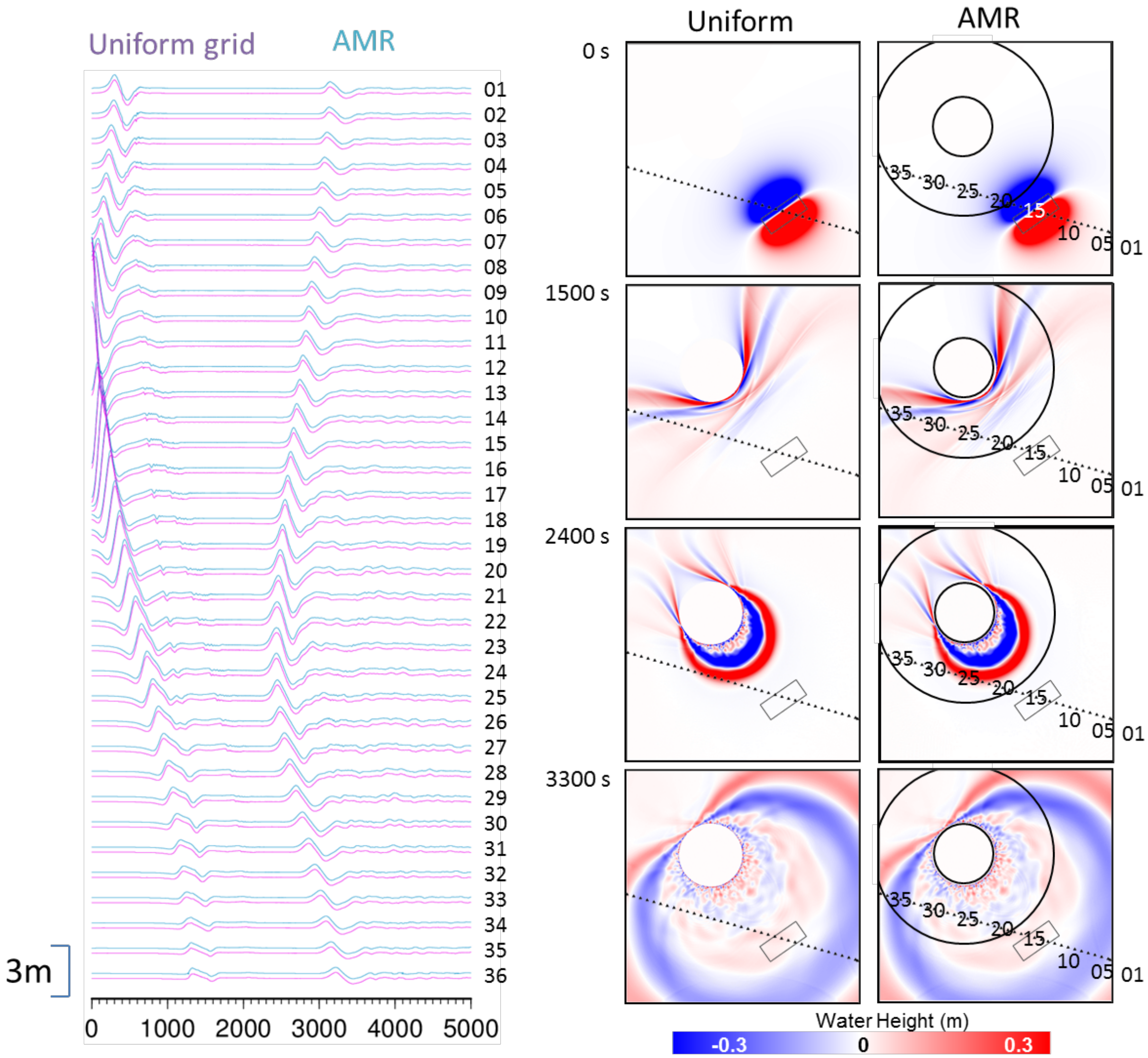

Fig. 6 Comparison of the tsunami simulation results between the AMR solver and conventional solver. Left: waveforms at stations shown in the right. Right: snap shot of the wave height.

Table 2 –Setting of source model

Parameters	value	Unit
Origin (X, Y, Z)	90000, -70000, 15000	m
strike, dip, rake	235, 11.1652, 90	degree
Length	61730	m
Width	25870	m
Slip	7.9	m

Table 3 – Condition for simulations

	AMR solver	Conventional solver	unit
Area (length)	327600	328050	m
The number of cell / level	216522 / 0, 34991 / 1	532900	cell
Grid spacing / level	450 / 0, 1350 / 1	450	m
Depth to bottom	10000		m
Time step	75000		step
Time interval	0.2		s
Calculation time	15383	17246	s

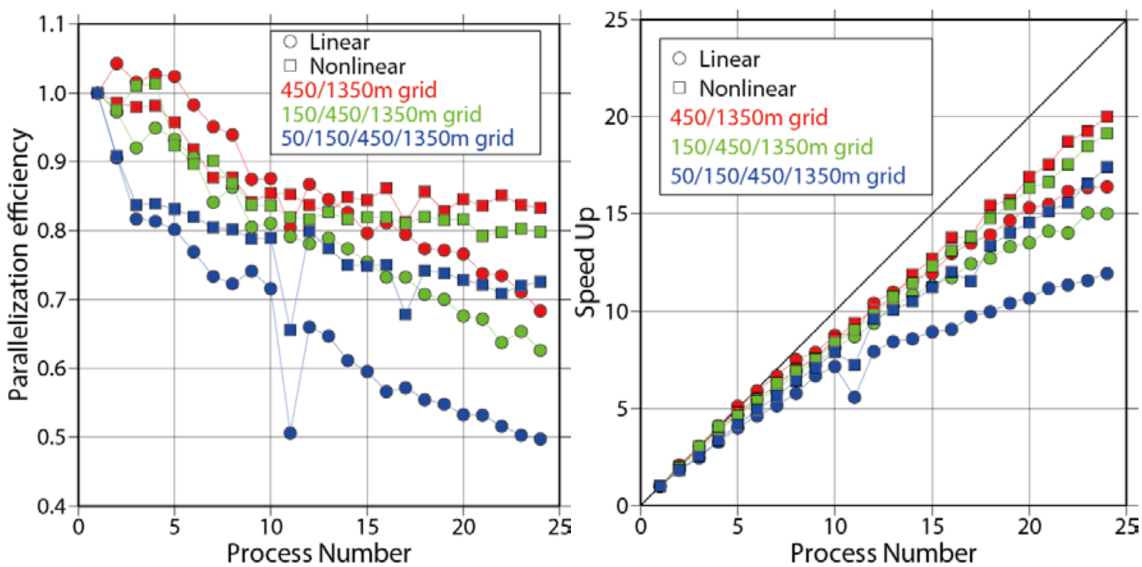

Fig. 7 Parallelization efficiency and speed up of linear and non-linear tsunami simulation.

Then, the performance test of parallel computing is conducted using nona-tree structured grid for the two, three, and four consolidation-level grids. The computing environment used in the performance test is shown in Table 4. Conditions of constructing adaptive meshes are shown in Table 5. The source model is shown in Table 6. For the case of the linear long-wave theory for two-level grids (450m/1350m), Fig. 7 indicates that the parallelization efficiency is larger than 100% up to 5 parallel-running tasks and is monotonically decreased at higher degree of parallelism and about 70% in the case of 24 parallel-running tasks. In the case of a non-linear long-wave theory, parallelization efficiency is close to 100% up to 5 parallel-running tasks and decrease to near 80% at higher parallel-running tasks. In the case of three-level grids (150m/450m/1350m), the parallelization efficiency for the linear long-wave theory and non-linear long-wave theory show slightly lower values than those for the two-level grids, respectively. In the case of four-level grids (50m/150m/450m/1350m), although the parallelization efficiency are lower than those for the three-level grids, the parallelization efficiency is still around 70% in the case of the non-linear long-wave theory calculating with 24 parallel-running tasks. In any consolidation levels, the parallelization efficiency for the non-linear theory is better than those for the linear theory. This is because the number of calculation with the non-linear theory is much larger than that with linear theory.

Table 4 –Computing environment

Compiler	Intel Fortran Composer XE 14.0.2.144
MPI	Intel MPI 4.1.3
CPU	Intel Xeon E5-2697v2（2.7GHz, 12core）
Memory (GB/node)	64
Interconnect	InfiniBand

Table 5 –Condition for evaluation

case	1	2	3
Factor of safety (α_{CFL})		10	
The number of grid cells	4768117	31155444	45535660
The number of consolidation level	2	3	4
Grid spacing (m)	450, 1350	150,450,1350	50,450,1350
Time interval (s)	0.2	0.1	0.02
Time step (steps)		1000	
The number of process		1-24	

Table 6 –Source model

Parameter	Value	unit
Top of fault plane	6755.73	m
Strike, dip, rake	191.63, 11.165, 90	degree
Length	317300	m
Width	158700	m
Slip	7.9	m

5. Conclusion

In this study, we developed a system to automatically generate an optimal mesh model based on the adaptive mesh refinement (AMR) method and a two-dimensional tsunami simulation code adapted for the AMR. By using a quad-tree and nona-tree structured grids, it was able to automatically create an adaptive mesh model based on the some conditions such as CFL condition. By using the nona-tree structured grid, we can directly use the bathymetry data constructed for the nesting. Developed simulation code was compared with the conventional tsunami calculation code using a uniform grid. The calculation result for the same bathymetry and source data showed good agreement. The number of grid cells was reduced by half by using AMR compared with the uniform grid. The calculation time was shortened approximately 10% using the AMR solver compared with that by the conventional solver. The performance test showed that the parallelization efficiency of non-linear long-wave theory for four consolidation-level grid model is around 70% in the case of 24 parallel-running tasks.

For further improvement in efficiency of calculation, we will adapt our tsunami modeling to GPGPU. Then, using the improved code, we will carry out many calculations using the linear tsunami modeling to extract source models that have a strong influence on tsunami height. Finally, we will carry out a heavy non-linear tsunami modeling to obtain tsunami inundation for the extracted source models.

6. Acknowledgements

This work was supported by Council for Science, Technology and Innovation (CSTI), Cross-ministerial Strategic Innovation Promotion Program (SIP), "Enhancement of societal resiliency against natural disasters"(Funding agency:JST).

7. References

[1] Popinet, S. and Rickard, G. (2007) : A tree-based solver for adaptive ocean modelling, *Ocean Modelling*, **16**, pp.224-249. doi:10.1016/j.ocemod.2006.10.002.

[2] Yasuda, H., and Hoshino T. (2011) : Computation of shallow water equation with hierarchical quadtree grid system, *New Phase of River Discharge Observation*, **2**, pp.1-11.

[3] Furuyama, S., and Maihara, Y. : High resolution & high performance tsunami run-up simulation, *Journal of Ecotechnology Research*, **17** (2), 2014, pp.79-83.

[4] Chiba, Y., Mori, N., Yasuda, T. and Mase, H. : Optimum scheme of adaptive mesh refinement for tsunami simulation, *Coastal Engineering Proceedings*, **1 (**34), 2014, doi: 10.9753/icce.v34.currents.11.

[5] Acuna, M. A., and Aoki, T. : AMR Multi-GPU accelerated tsunami simulation, *in Proc. of the 32th JSST International Conference on Simulation Technology*, Tokyo, Feb 4, 2014.

[6] Imamura F., Yalciner, A. C., and Ozyurt G. : Tsunami modeling manual, UNESCO Tsunami modeling course (UNESCO), 2006.

[7] Okada, Y. : Internal deformation due to shear and tensile faults in a half-space, Bull. Seism. Soc. Am., Vol.82, 1992, pp.1018-1040. Vamvatsikos D, Cornell CA (2002): Incremental dynamic analysis. *Earthquake Engineering & Structural Dynamics*, **31** (3), 491-514.